Safe Li-Ion Batteries Using Electrode Coated Silicalite Separators For Improved Performance And Cycle Life

by

Dheeraj Ram Lingam Murali

A Thesis Presented in Partial Fulfillment
of the Requirements for the Degree
Master of Science

Approved April 2022 by the
Graduate Supervisory Committee:

Jerry Lin, Chair
Christopher Muhich
Cesar Torres

ARIZONA STATE UNIVERSITY

May 2022

ABSTRACT

Lithium-ion batteries are widely used for high energy storage systems and most of the commercially manufactured lithium-ion batteries use liquid electrolytes and polymeric separators. However, these electrolytes and polymeric separators pose safety issues under high temperatures and in the event of short circuit which may lead to thermal runaway and cause fire. The application of fire-retardant high salt concentrated electrolytes can be used to address the safety issues that arises in the use of liquid electrolytes, but these electrolytes have high viscosity and low wettability when used on polymeric separators which are commercially used in lithium-ion batteries. To address this issue, zeolite powder has been synthesized and separators were prepared by coating on the electrode using scalable blade coating method. Zeolite separators have higher wettability and electrolyte uptake compared to polymeric separators such as polypropylene (PP) due to their intra-particle micropores. The zeolite separators also have higher porosity compared to PP separators resulting in higher electrolyte uptake and better electrochemical performance of the lithium-ion batteries. Zeolite separators have been prepared using spherical-silicalite and plate-silicalite to analyze the effect of morphology of the particles on the electrochemical performance of the cells. The plate-silicalite separators have higher capacity retention during long-term cycling at low C-rates and better capacity performance at high C-rates compared to spherical-silicalite. Therefore plate-silicalite is very promising for the development of high-performance safe lithium-ion batteries.

ACKNOWLEDGMENTS

Firstly, I would like to express my gratitude to my parents for providing me with love and encouragement throughout my education. Your support and help in guiding me have made me take the right decision and work hard to achieve my goals.

I would like to thank my advisor, Dr. Jerry Lin for his mentorship and guidance. Thank you for providing me with an opportunity work on Lithium-ion batteries despite not having any research background. I have learned valuable knowledge and skills which will help me in my career under your patient and careful guidance.

I would like to thank Dr. Christopher Muhich and Dr. Cesar Torres for their willingness to serve on my committee and their valuable comments.

Lastly, I would like to thank the members of Dr. Jerry Lin's group. I would like to thank Dr. Kishen Rafiz, Dr. Oscar Ovalle Encinia and Fateme Benihashemi for who have been helpful during my time working alongside them. I would like to thank Fred Pena for fixing issues that arises in the lab.

TABLE OF CONTENTS

Page

APPENDIX Page

LIST OF TABLES

Table Page

LIST OF FIGURES

CHAPTER 1

INTRODUCTION

1.1 Lithium-ion/metal battery

Lithium-ion batteries have high energy density (250-680 Wh/L), high specific energy (100-270 Wh/Kg), low self-discharge rate, long cycle life and a broad temperature range of operation which makes it the preferred method of energy storage in recent times and are used in electronic devices, electric vehicles etc. [1][2]. The lithium-ion batteries which are used commercially are secondary cells made of electrodes coated on current collectors, an electrolyte which conductive of lithium ions and a separator which is electronically insulating.

The commonly used cathodes are Lithium Cobalt oxide (LCO), Lithium Manganese oxide (LMO) and Lithium Nickel Manganese Cobalt oxide (NMC). While Graphite is the most preferred material used as an anode [3]. The electrolytes used in commercial batteries are mostly liquid electrolytes as they have good ionic conductivity and low internal resistance. The most used electrolytes are lithium salts dissolved in organic solvents such as LiPF6 dissolved in a mixture of Ethylene Carbonate (EC), Diethyl Carbonate (DEC) and Dimethyl Carbonate (DMC) at different ratios. The separator is porous material which has good electrolyte wettability and electrolyte uptake. Separators such as polymeric separators which are very thin and have good porosity are widely used in Lithium-ion batteries [4].

Lithium has the highest theoretical capacity of 3860 mAh/g and less density. This makes lithium one of the desirable materials for anode and a motivation in the development of lithium metal batteries [5]. However, the usage of lithium metal batteries

has its own challenges due to the formation of lithium dendrites which could short circuit the battery leading to thermal runaway [6][7].

1.2 Literature Review

The recent increase in the use of Lithium-ion batteries has also posed a problem on the safety issue as there have been multiple reports of fire and explosion [8][9]. Studies have reported that the thermal runaway mechanism in Li-ion batteries is the chain reaction of an uncontrollable temperature increase [10][11]. Heat is normally generated due the electrochemical reaction inside the battery. The heat is nominally dissipated as it is generated during the cycling of the battery. However, if the battery is subjected to abuse such as overcharging, external heating and penetration then the heat is generated excessively compared to normal operation conditions [12][13][14]. Then the excessive heat generated cannot be dissipated using natural heat dissipation which would then lead to increase in the internal temperature of the battery [15].

The components of the battery tend to decompose as the internal temperature rises. The decomposition of the solid electrolyte interface (SEI) on the anode electrode occurs around 80^{o}C, the electrolyte usually starts to breakdown at around 100-120^{o}C and the collapse of separators such as polymer separators is around 135^{o}C [16][17][18]. Once the electrolyte breaks down, flammable hydrocarbon gases, including H_2, CH_4, C_2H_6, and C_2H_4, are generated and may be ignited at a high temperature and if the separator collapses then internal short circuit may occur which would lead to even more gnereation of heat [19][20]. These side reactions aggravate the abnormal temperature increase, in turn, promote the chain reactions until thermal runaway occurs.

The widely used polymeric separators have poor mechanical stability at relatively high temperatures above 90^{o}C and organic carbon-based electrolyte easily decomposes at high temperature and are flammable [21]. Hence, the need for the development of non-flammable electrolyte and separators that thermally stable at high temperatures with better performance. Since most of the Li-ion batteries use liquid electrolytes, there have been recent development in the study of flame retardant electrolytes for safe Li-ion batteries but have been unsuccessful due to either the cooling effect realized by the vaporization of the solvent or the inability to form stable passivation layer [22][23].

Conventional electrolytes are mostly composed of lithium hexafluorophosphate (LiPF6) dissolved in a mixture of ethylene carbonate (EC) and linear carbonates [24]. Carbonates have high volatility and flammability. However, the high flammability of linear carbonates, such as diethyl carbonate (DEC), dimethyl carbonate (DMC), and ethyl methyl carbonate (EMC), is the biggest safety concern of lithium-ion batteries [25].

Solvents like Adiponitrile (ADN) is considered as a safe electrolyte because it is chemically stable and has a high boiling and flash point and low vapor pressure. ADN was used as a single-electrolyte solvent with lithium bis(trimethylsulfonyl)imide (LiTFSI) since it exhibits high electrochemical stability, indicating its potential as a suitable electrolyte for safer Li ions cells without compromising the performance [26]. Trimethyl phosphate (TMP) was used as a solvent because it is identified as a good flame retardant and has high oxidative stability and low viscosity and it can form stable solid electrolyte interface (SEI) [27][28]. Salt concentrated electrolytes have been used with fire retardant solvents have shown good performance and stable charge-discharge cycles of the batteries. Salts such as lithium tri-sulphonyl imide (LiTFSI), Lithium

bis(oxalate)borate (LiBOB) and lithium bis-(fluorosulphonyl) imide (LiFSI) are used to develop high concentrated electrolytes where the concentration of the salt is greater than 3M [29].

The study of the performance of the salt concentrated electrolytes using LiFSI salt and TMP without any additives or binders has shown great improvement in the flame retardant nature as well as long cycle life due to the formation of stable SEI associated with the high concentration of lithium fluoride (LiF), which also reduces the possibility of dendrite formation at the anode [28][29]. Salt concentrated electrolytes have high viscosity which greatly affects its ability to wet commercial polymeric separators as they low surface energy and low porosity. This results in slow wettability and non-uniform diffusion of the electrolyte affects the battery cycle life and increase in the battery production time [30].

The polymeric separators a large thermal shrinkage at temperatures above 90^{o}C. This increases the chance of an internal short circuit and thermal runaway at elevated temperatures [31]. Combined with the low porosity and poor robustness of the material makes it impractical for the manufacture of salt concentrated electrolyte-based Li-ion batteries. In order to address the issue of the thermal stability and electrolyte wettability of the polymeric separators, inorganic materials such as alumina, silica and zeolites have been studied as a solution to improve the limitations of the commercially available polymeric separators [32].

Inorganic materials have surface energy and high wettability and their exceptional mechanical stability over a wide range of temperatures makes them a good substitute for polymeric separators [33]. A popular approach to increase the wettability and the thermal

stability of the polymeric separator is to mix the inorganic materials with a binder and coat them on the polymeric separator. Silica and alumina are few of the popular ceramic powders used for the coating due to its low cost [34].

A novel membrane based on silicon dioxide (SiO_2) and hydroxypropyl guar gum (HPG) as binder is used to coat the polymeric separator giving high wettability and thermal stability to the separator [35]. Another case study of using a high MP poly(vinyl alcohol) (PVA) binder for ceramic coating (Al_2O_3) of polyolefin separators has been performed to improve the thermal stability of the separator [36]. A comparative study on coating a commercial polypropylene separator with four inorganic materials, i.e., Al_2O_3, SiO_2, ZrO_2 and zeolite shows that all inorganic coatings have improved thermal stability with differences in the electrical resistance but have similar cell performance as the pure polymer separator [37]. However, the bulk of the separator is still polymeric so there is a high chance of combustion in case of thermal runaway.

The use of polymer free inorganic separators is used to overcome this problem. Free-standing separators have been successfully reported using sintered Al2O3 and SiO2 powders [38][39]. The issue with these separators were with their brittle nature resulting in the need to make thick separators (~200 µm) which increases the cell's internal resistance and decreases the energy density. There have further studies on decreasing the thickness of the free-standing inorganic separator, but they require large amounts of binder, or the synthesis procedure of the separator is complex and chemically intensive [40][41].

Recently, a new method of inorganic separator preparation has been reported using the blade coating technique to coat alumina powder directly on the electrode by

preparing an alumina slurry and coating the slurry to obtain a thin (~40 μm) alumina separator [42]. Polymer free electrode coated separators with alumina and quartz silica powders have prepared using blade coating method and their cell performance have been studied [43]. These separators have shown excellent electrolyte wettability and better thermal stability and electrochemical performance of the cell and are easily scalable providing a better choice for the commercial manufacturing process [44][45].

1.3 Research motivation and objective

The inorganic separators prepared using alumina and silica powders have higher density compared to polymeric separators resulting in lower energy density of the cell. However, these metal oxides are dense particles, and the lithium-ion transport occurs only via the inter-particle pores which makes the lithium ions localized to a specific spot rather than distributed homogeneously leading to non-uniform SEI formation. Microporous particles such as zeolites which has good wettability towards salt concentrated electrolytes and better thermal stability. Recently silicalite have been used coat the separator on cathode and their performance has been compared with silica and PP separators using salt concentrated electrolytes [46]. Here we report the study of blade coated and electrode supported porous silicalite (MFI type zeolite) separators of different particle morphologies and its effect on the internal resistances and the performance of cell rate capability and its capacity retention.

1.4 Thesis structure

The objective of the research is to synthesize silicalite powders of two different morphologies such as spherical silicalite and plate silicate and analyse its effect in cell performance. Here we synthesize spherical silicalite and plate silicalite powders using the

hydrothermal process. The obtained silicalite powders were analysed using scanning electron microscope, mercury porosimeter and X-ray diffraction techniques. The silicalites are then used to prepare a slurry and the slurry is coated on the electrode using the blade coating method which is easily scalable. Standard coin cells were then assembled using both silicalite separators and using high concentrated salt electrolyte. The cell performance test such as charge-discharge, rate capability, long term cycle life and electrochemical impedance spectroscopy were conducted for both the silicalite separators.

CHAPTER 2

STUDY ON THE PERFORMANCE OF FULL LITHIUM-ION CELL USING SILICALITE SEPARATORS

2.1 Introduction

Silicalites are crystalline microporous silicates with periodic arrangements of cages and channels that find extensive industrial uses as catalysts, adsorbents, and ion exchangers [47]. Silicalite films have been targeted for potential applications as selective membranes offer outstanding potential for molecular recognition at the subnanometer level and the ability to operate at high temperatures [48][49]. Silicalite particles have been synthesised using the hydrothermal process and oriented supported zeolite films of siliceous ZSM-5 ($[Si_{96}O_{192}]$-MFI) with superior performance have been focused because ZSM-5 has a channel system with pore openings and an excellent model system for fundamental studies on achieving preferred orientation in silicalite films [50][51].

As mentioned earlier, porous silicalite particles have been studied on the feasibility to be used as a separator the silicalite powder has been successfully coated on cathode material directly using the scalable blade coating method [46]. The particles synthesised are ~2 μm in size and are spherical in nature. The electrochemical tests of the cell constructed using the porous silicalite separator and high concentrated salt electrolyte has shown better performance as compared to cell constructed using silica and PP separator. In this section of the study, we focus on the effect of the morphology of silicalite separator coated using spherical silicalite and plate silicalite on the performance of the cell.

2.2 Experiment

2.2.1 Preparation of silicalite powders and electrolyte synthesis

The silicalite (pure silica MFI type zeolite) was prepared using the hydrothermal synthesis method. Silicalite has microporous porosity of 39% and crystal density of 1.76 g/cc [52][53]. Spherical silicalite was prepared using 10 g of tri-ethyl orthosilicate (Millipore Sigma), 12 g of tetra-propyl ammonium hydroxide (Millipore Sigma) and 202 g of de-ionized water and were stirred in a beaker for ~20 hours at room temperature till a clear solution was obtained. The solution was then heated at 130^{o}C for 8 hours in an autoclave to obtain spherical particles of silicalite of size ~2 µm. While plate silicalite was prepared using 10 g of tri-ethyl orthosilicate (Millipore Sigma), 4 g of tetra-propyl ammonium hydroxide (Millipore Sigma) and 170 g of de-ionized water and were stirred in a beaker for ~20 hours at room temperature till a clear solution was obtained. The solution was then heated at 155^{o}C for 10 hours in an autoclave to obtain plate particles of silicalite of size ~3 µm.

Next the mother liquor was decanted from the autoclave after the completion of the reaction and cooled at room temperature. The obtained silicalite powders were washed by mixing it with de-ionized water and centrifuging the mixture at 5000rpm (16.8 relative centrifugal force – meters) for 20 minutes separately. This step needs to be repeated three to four times for both silicalite powders to completely remove the organic components present in the powders post reaction. Both washed silicalite powders were then dried at 100^{o}C in a vacuum oven for 24 hours to remove the moisture from the powders. This was followed by calcination of the powders at 600^{o}C in a furnace for 10 hours. This synthesis method was adapted and modified from literature [46][54].

The cathode used was $LiNiCoMnO_2$ (5:2:3) of thickness 45µm coated on aluminium foil and the anode used was graphite of thickness 50µm coated on copper foil and the electrode materials were procured from MTI Corporation. The lithium bis-fluoro sulphonyl imide (LiFSI) (battery grade) salt was procured from Kishida Chemical Corporation, Japan, and the tri-methyl phosphate solvent (TMP) (reagent grade; 99.999% purity) was procured from Millipore Sigma. The required weight of LiFSI salt and TMP were mixed to obtain a salt concentrated clear liquid solution of 5.3M inside an atmosphere-controlled glovebox (H2O < 0.1 ppm, O2 < 0.1 ppm) and the obtained solution was allowed to rest for 24 hours.

2.2.2 Coating of silicalite separators and characterization

The preparation of slurry using silicalite powder is required to coat the silicalite on the NMC cathode. The slurry was prepared by mixing 5 g of spherical silicalite powder with 0.5 g of 5 wt.% polyvinyl alcohol (PVA) aqueous solution (molecular weight: 77 000– 79 000) (ICN Biomedical Inc., USA) and 2 g de-ionized water. For plate silicalite the slurry was prepared by mixing 2 g of plate silicalite powder with 2 g of 5 wt.% polyvinyl alcohol (PVA) aqueous solution (molecular weight: 77 000– 79 000) (ICN Biomedical Inc., USA) and 1 g de-ionized water. The mixture was stirred for ~10 minutes to obtain a homogeneous slurry. The coating of the slurry on the electrode was done by using a caliper-adjustable doctor blade (Gardco LLC, USA). For the coating of the silicalite separator of desired thickness, the blade gap was adjusted to 40 µm. The prepared slurry was then dropped across one end of the electrode and then spread down the length of the electrode using the doctor blade to obtain a uniform coating. The coated separator was dried in a humidity-controlled chamber at 40^{o}C and 60% relative humidity

for 10 hours. These blade coating steps were followed to coat both the spherical and plate silicalite separators.

The morphology and the cross-section of the prepared silicalite separators were observed using scanning electronic microscopy (Philips, USA, FEI XL-30) and the samples were prepared by sputter-coating them with gold. The porosity of the separator was measured based on the density of the particle and measured bulk density (using the weight and dimensional volume of the coated silicalite separator). The tortuosity of the separators was measured using the conductivity of the electrolyte, porosity of the separators and the conductivity of the separators ($\tau = \sigma_{el}\ \varepsilon/\sigma$). X-ray diffraction patterns were obtained (Bruker AXS-D8, Cu Ka radiation, USA) for both silicalite powders and silicalite separators coated on NMC to analyse the phase structure of the silicalite particles. The silicalite particles were coated on the aluminium foil and were cut into square sheets of 3 cm by 3cm after drying them. These sheets were used to measure pore size distribution of the interparticle pores of the silicalite separators using a mercury porosimeter (Micrometrics Auto Pore V, USA) and the Porosimetry was performed at both the h high-pressure mode and low-pressure mode to detect pore sizes ranging from nanometer to micrometer dimensions. The contact angle measurement was done to both silicalite particles coated on the aluminium foil and PP separator by dropping the 5.3 M LiFSI/ TMP electrolyte on a DSA-25 Drop Shape Analyzer (Kruss, USA) at intervals of 1 second and recording them as images.

2.2.3 Cell assembly and electrochemical characterization

The electrode coated silicalite separators were cut into 16mm diameter discs using the disc cutter (MTI Corporation) and the cut discs were kept in a vacuum oven at 70^{o}C

for 12 hours. The obtained discs were then immediately placed inside an argon-filled glovebox (Innovative Technology Inc., USA) and kept in it for a period of 24 hours to remove any traces of atmospheric gases or moisture in the electrode-supported separator disks. The coin cells assembled were using the CR2032 type coin cells (X2 Labwares, Singapore) and inside the glovebox. The cut discs of electrode coated separator was first placed inside the bottom case of the coin cell and the prepared 5.3M LiFSI/TMP electrolyte of 150 µl was pipetted out onto the surface of the silicalite coated NMC cathode. Graphite anode of 16mm was then placed on top of the separator surface and followed by two spacers and one spring. Finally, the top case of the coin cell was placed to enclose the coin cell. The coin cell was then crimped at 400psi to seal the coin cell. This procedure was used to construct coin cells for both electrode coated silicalite separators.

The constructed coin cells were then removed from the glovebox and the charge-discharge characteristics of the cells was tested using NEWARE battery testing system (BTS3000) (Neware Co, Shenzen, China). The cells were cycled using the standard CC–CV (constant current– constant voltage) method where the minimum and maximum potential for testing were 2.0 volts and 4.2 volts respectively. The cells prepared using both spherical and plate silicalite separators were first tested at 0.2C-rate for 100 cycles to test the cycle life performance the cells. Subsequently the cells were cycled at higher C-rates of 0.5C, 1C and 2C to test the rate capability of the cells using spherical and plate silicalite separators. Electrochemical impedance spectroscopy (EIS) measurements of the assembled cells were conducted using a PARSTAT 2263 EIS station (Princeton Applied Research, USA) in the AC mode to analyse the internal resistance of the cells. The

Nyquist plots were obtained for the assembled cells (100% SOC) were generated by utilizing a frequency range of 100 kHz to 10 mHz and d an AC amplitude of 10 mV rms. All the electrochemical tests for both spherical silicalite and plate silicalite separators were performed at room temperature.

2.3 Results and Discussion

Silicalite (MFI type zeolite) has good chemical and thermal stability and lower density compared to other metal oxides which makes it a good substitute for polymer separators. Silicalite has been previously used to prepare separators by coating them on the NMC cathode through blade coating method and this separator has shown better electrochemical performance and better thermal stability compared to polymer separators [21]. Here we report the use of spherical silicalite and plate silicalite as separators and study their electrochemical performance.

Silicalite powders of spherical shaped and plate shaped were synthesised using the hydrothermal process from tri-ethyl orthosilicate with tetra-propyl ammonium hydroxide as the organic template. The silicalite powders were mixed into an aqueous solution using polyvinyl alcohol (PVA) as the binder and the slurry was coated on the NMC cathode to obtain a coating of the silicalite separators of 40 μm thickness. The PVA added to slurry mixture is reduced to a minimum level so to avoid it affecting the electrochemical performance of the cell. The final coating thickness of the silicalite separators is 30 μm in thickness after they undergo the drying process. The spherical silicalite gives a relatively smooth coating as shown in Figure 2.1(a) as compared to plate silicalite which gives a coarse coating as shown in Figure 2.1(b). This difference in the coating texture is due to the morphology of the particles as spherical particles give a good

particle packing when coated using the blade coating method as compared to plate silicalite particles which would need external pressure to obtain a smooth surface.

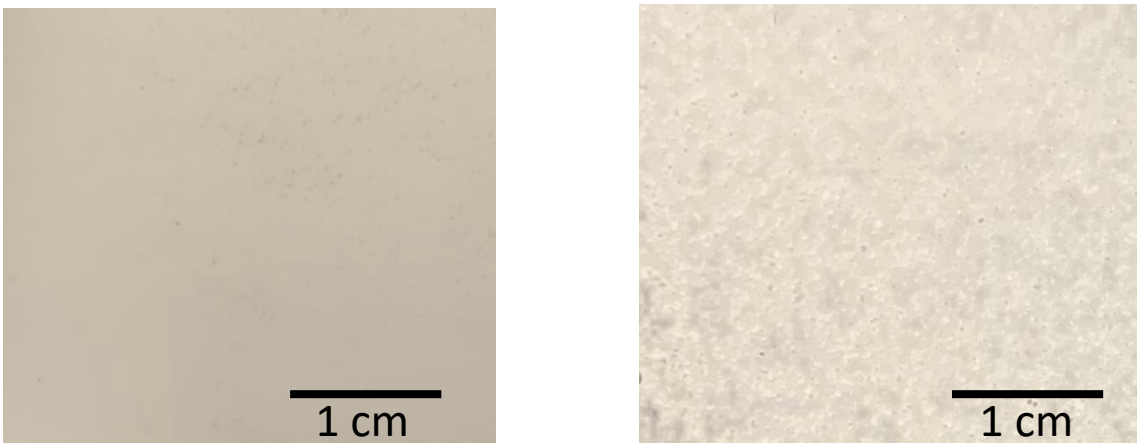

(a) (b)

Figure 2.1. Optical images of (a) Coating of spherical silicalite on top of NMC cathode. (b) Coating of plate silicalite on top of NMC cathode.

The coated silicalite separators were used to prepare samples by sputter coating them with gold for the scanning electron microscope (SEM) images. Figure 2.2(a) shows the SEM images of the surface view of the plate silicalite particles and the cross-sectional view of the plate silicalite layer coated on NMC cathode. The surface view shows the morphology of the plate structure of the silicalite, and the average particle size is in the range of ~3 μm(length) and ~500nm(thickness) and the aspect ratio of length to thickness is 6 and the cross-sectional view shows the plate silicalite layer coated on the NMC layer. Similarly Figure 2.2(b) shows the SEM images of the surface view of the spherical silicalite particles and the cross-sectional view of the spherical silicalite layer coated on NMC cathode. The surface view shows the morphology and the size of the spherical silicalite particles which is spherical and the average particle size of ~2 μm in size and the cross-sectional view shows spherical silicalite layer coated on the NMC Cathode.

Both spherical and plate silicalite separator layer are ~30 µm in thickness which confirms the reduction in the coating thickness of the separator layer due to drying process in the humid chamber followed by drying in vacuum oven.

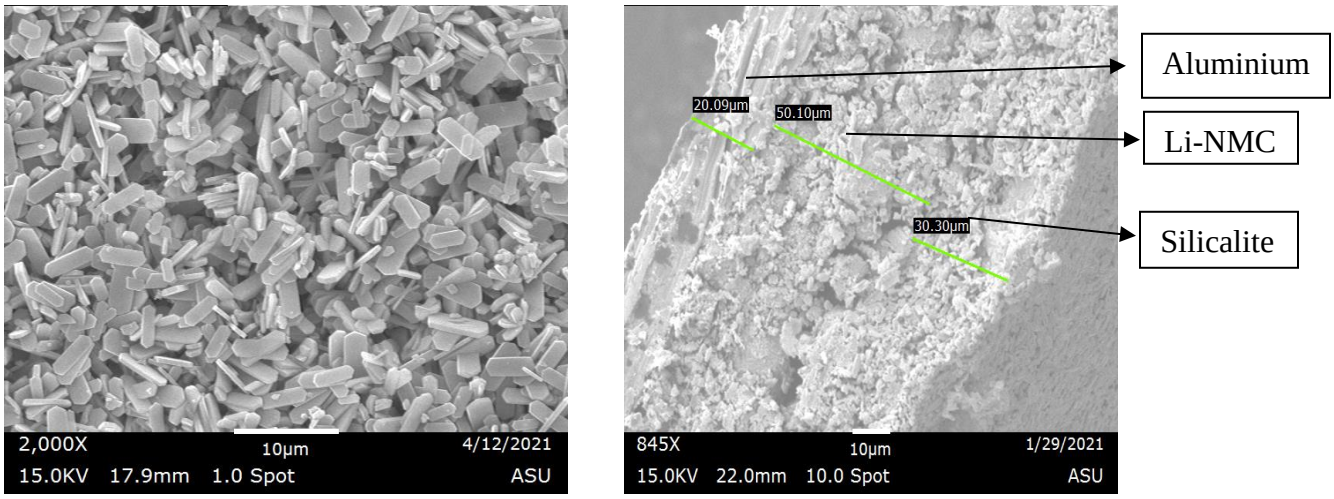

(a)

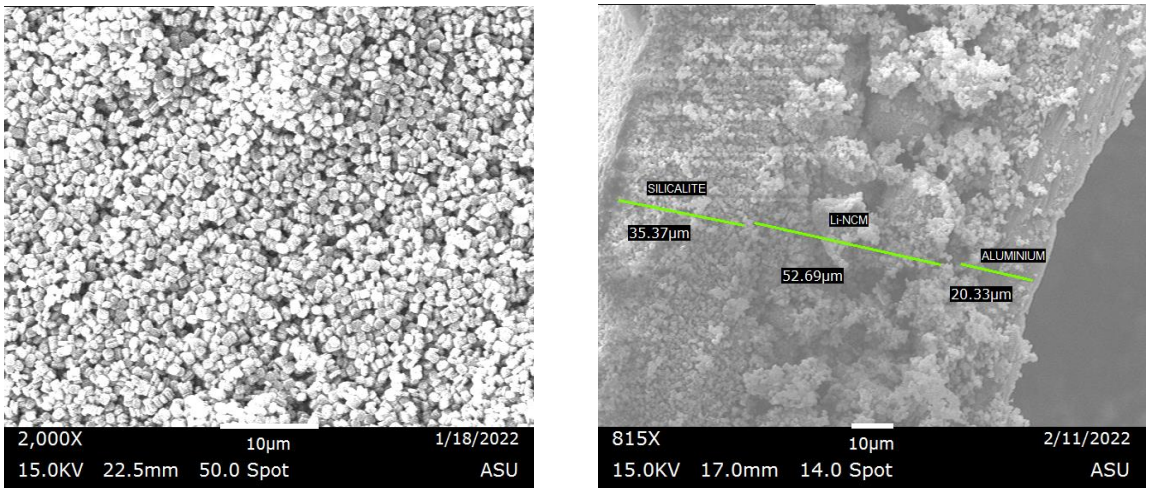

(b)

Figure 2.2. SEM images of plate silicalite and spherical silicalite. (a) Surface view of plate silicalite particles (left) and cross-sectional view of the plate silicalite coated on NMC cathode (right). (b) Surface view of spherical silicalite particles (left) and cross-sectional view of the spherical silicalite coated on NMC cathode (right).

A comparison of the morphology of the two silicalite particles as shown in Figure 2.2(a) and (b) shows that they are similar in particle size, but the shape of the particles is different as spherical silicalite are more rounded in shape whereas plate silicalite are nearly cuboid in shape. These silicalite particles of sizes 2-3 μm in size gives good adhesion of the silicalite particles when coated using the blade coating method on the NMC cathode particles whose particle pores are in the same size range as it has been previously established in the literature for the electrode-coated porous ceramic separators by the blade-coating method [43]. Silicalite powders were coated on aluminium foil for the analysis of mercury Porosimetry and the pore size distribution of the spherical silicalite separator and plate silicalite separator were obtained. Figure 2.3(a) and (b) shows the results of the pore size distributions of spherical silicalite separator and plate silicalite separator respectively. Figure 2.3(c) shows the particles of plate silicalite and spherical silicalite. As we can see, the plate silicalite separator and spherical silicalite separator have similar pore size but due to the morphology of the particles plate silicalite has higher tortuosity and lower porosity while spherical silicalite has higher porosity and lower tortuosity.

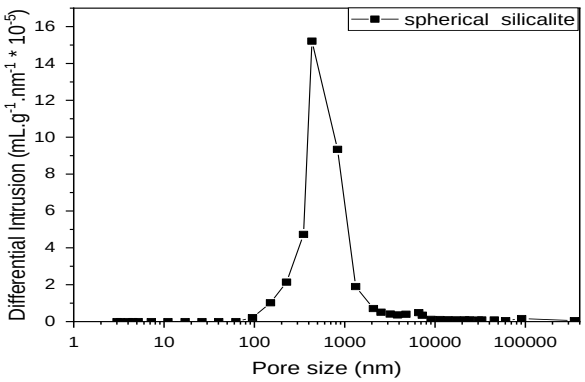

(a)

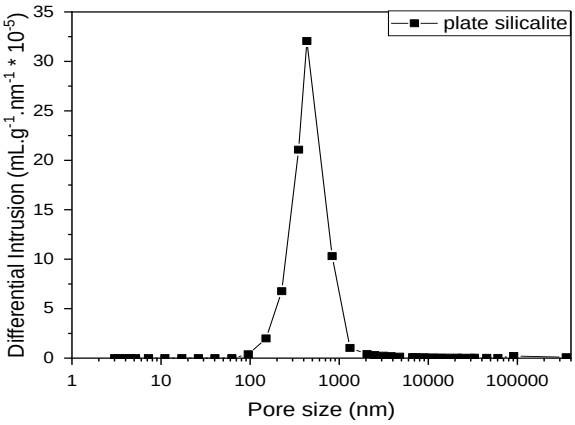

(b)

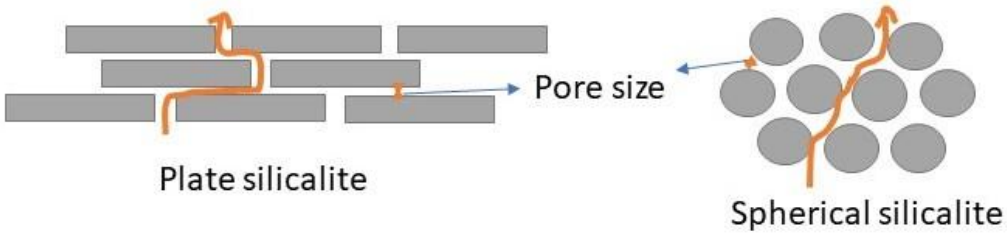

(c)

Figure 2.3. Inter-particle pore size distribution of (a) spherical silicalite separator and (b) plate silicalite separator (c) images showing the pore gap between the particles of plate silicalite and spherical silicalite.

Salt concentrated electrolyte of 5.3M lithium bis-fluoro sulphonyl imide (LiFSI) in tri-methyl phosphate solvent (TMP) was prepared for the study of the safe Li-ion cells as they have fire retardant properties. To show the wettability of the prepared silicalite separators and compare them with the commercially obtained PP polymer separator, a single sessile drop wettability test was performed. The prepared liquid salt concentrated 5.3M LiFSI/TMP electrolyte is dropped against the separators to measure the contact angle. Figure 2.4 shows the contact angle measurements of the silicalite and PP

separators as a function of time. The contact angle decreases much faster for silicalite separators as compared to PP separators due to the microporous nature of the silicalite particles and higher surface energy of the inorganic separators which results in better electrolyte uptake and wettability. Even though both silicalite separators are microporous in nature the spherical silicalite separator has relatively lower contact angle because it has higher porosity and lower tortuosity compared to plate silicalite separator.

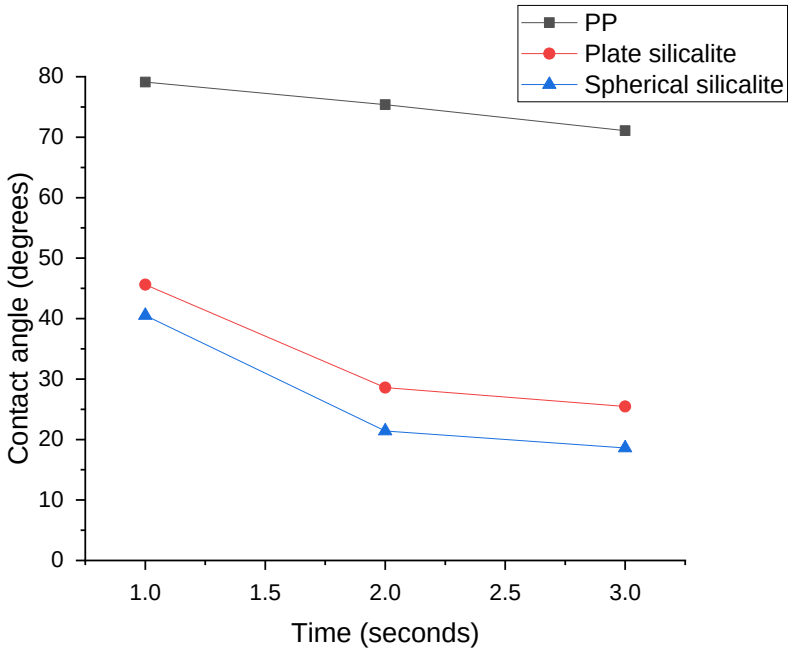

Figure 2.4. Change in the contact angle with time for PP, plate silicalite and spherical silicalite showing the wettability of LiFSI/TMP electrolyte.

The X-ray diffraction (XRD) analysis of the silicalite separators were performed to confirm the characteristics of the silicalite powders and the coated silicalite separators. Figure 2.5(a) and (b) shows the XRD pattern for the silicalite powder, silicalite separator coated on NMC cathode and silicalite separator compressed at 400 psi of spherical silicalite and plate silicalite respectively. The XRD pattern of the plate silicalite shows

that the particles are oriented with the plate area facing the top while there is no significant change in the orientation of the spherical silicalite particles. This phenomenon is observed because the length to thickness aspect ratio is 6 and due to the compression the silicalite particles align themselves such that the micropores of the particles (200 plane) is in the perpendicular orientation to plate face area which makes micropores are facing the electrodes. This allows the propagation of the solvated lithium ions to diffuse along the pores in the direction of (200) plane between the electrodes during charge-discharge cycle.

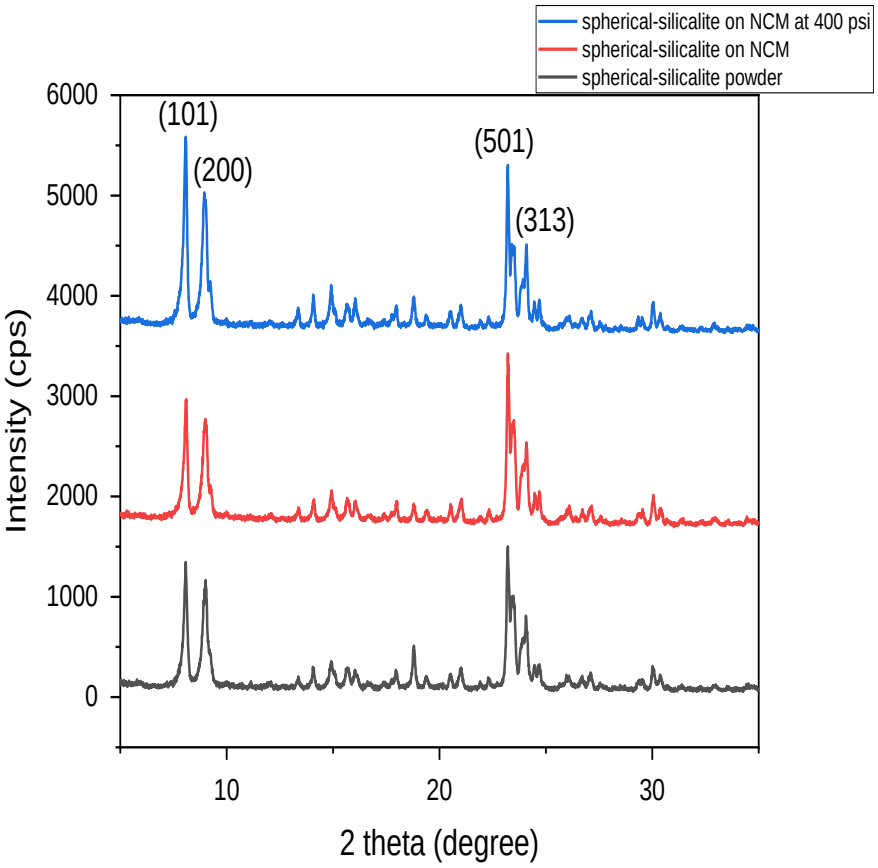

(a)

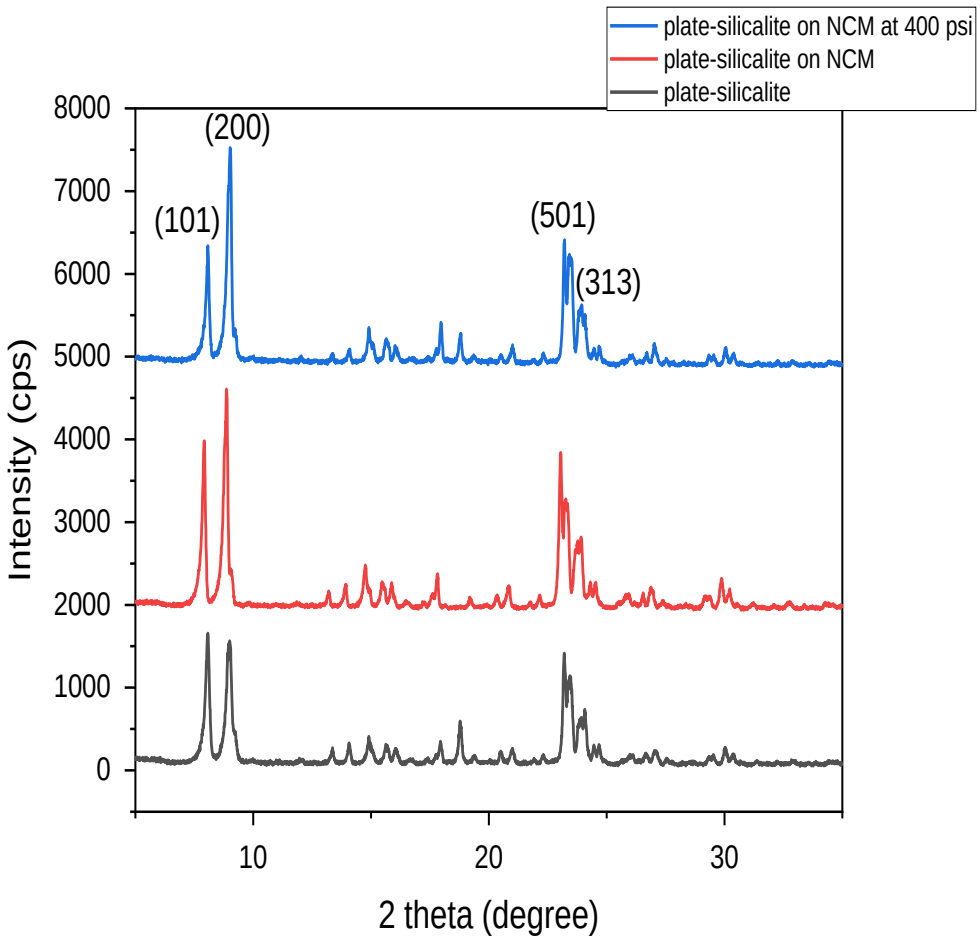

(b)

Figure 2.5. XRD pattern of silicalite powder, silicalite coated on NMC and silicalite separator compressed at 400 psi of (a) spherical silicalite and (b) plate silicalite.

The SEM images shown in Figure 2.6 confirms with the XRD pattern which shows the silicalite separator before and after compression of spherical and plate silicalite. This shows that plate silicalite separator undergoes further realignment and packing of the particles after crimping of the cell due to their non-uniform structure making the separator more tortuous. While spherical silicalite particles do not change significantly under the application of pressure due to the uniform morphology of the particles and thus no significant change the separator tortuosity. This gives two silicalite

separators with similar pore size distribution but different particle morphology and tortuosity. The porosity of the plate silicalite is lower than spherical silicalite and its higher tortuosity confirms with the results shown in the contact angle measurement as spherical silicalite is loosely packed and more porous making it uptake electrolyte faster.

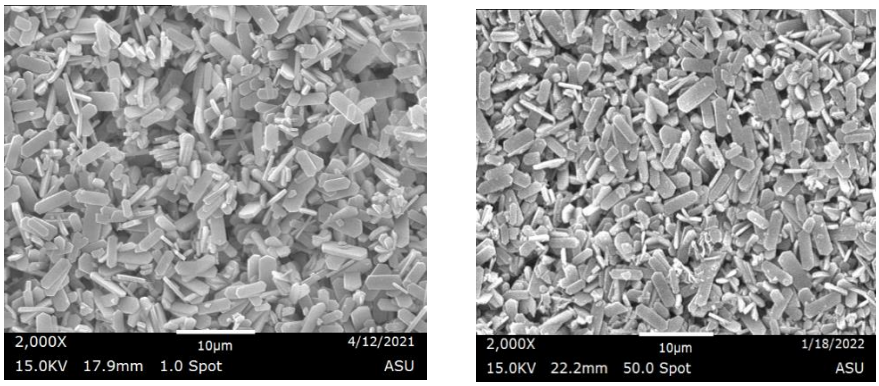

(a)

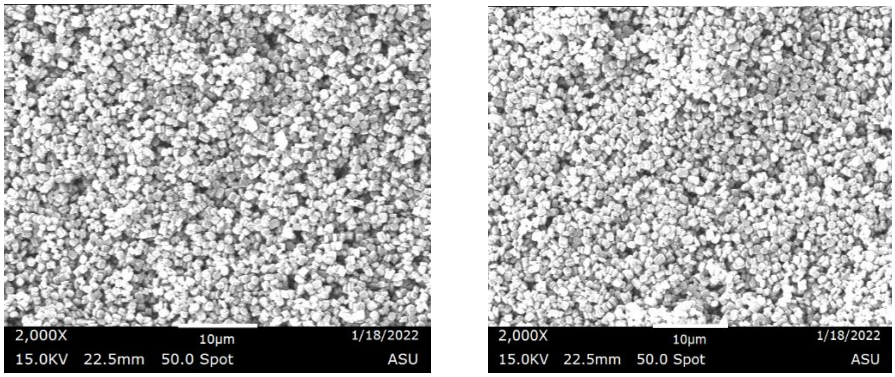

(b)

Figure 2.6. The SEM images of silicalite separators before and after compression at 400 psi of (a) plate silicalite and (b) spherical silicalite.

In previous studies, full cells constructed using NMC/graphite as electrodes with silicalite, silica and PP separators filled with 5.3M LiFSI/TMP electrolyte were tested for their electrochemical performance and silicalite separator has shown significantly better performance in terms of capacity retention and rate capability [21]. In this study, full cells

were constructed using graphite as anode and NMC coated with spherical silicalite and plate silicalite as separators and the electrochemical tests such as cycle life and rate capability were performed. The cells were cycled using the CC-CV charge-discharge method. Figure 2.7(a) shows the charge and discharge curves of the 1st cycle and the 100th cycle for both silicalite separators cycled at 0.2C-rate. The charge-discharge curves for both cells are similar as both spherical silicalite and plate silicalite are microporous particles. However, the plate silicalite separator shows better capacity retention compared to spherical silicalite due to the uniform diffusion of the solvated li-ions through the intra-particle pores of the plate silicalite separator and easier access to the anode layer [25][26]. This results in the more uniform and thin SEI layer formation as compared to spherical silicalite resulting in fewer loss of active lithium ions and better coulombic efficiency of the plate silicalite separator as shown in Figure 2.7(b).

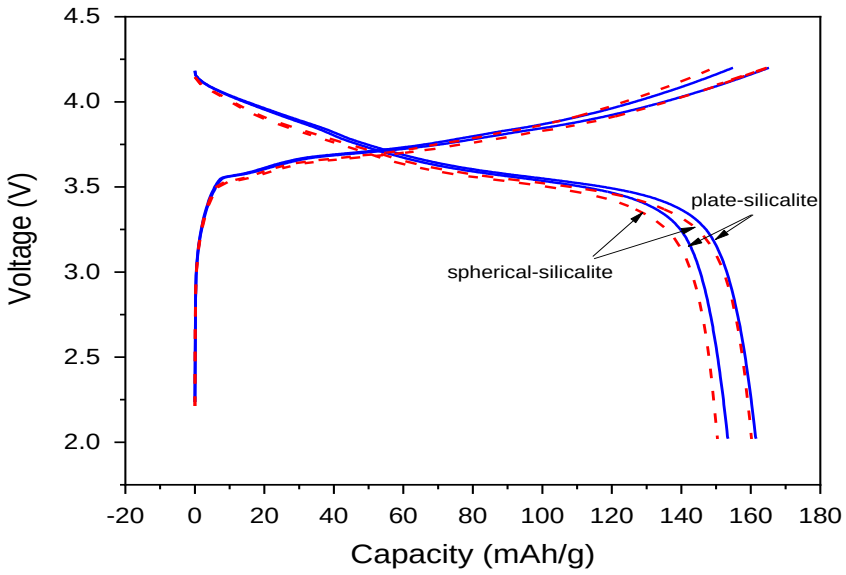

(a)

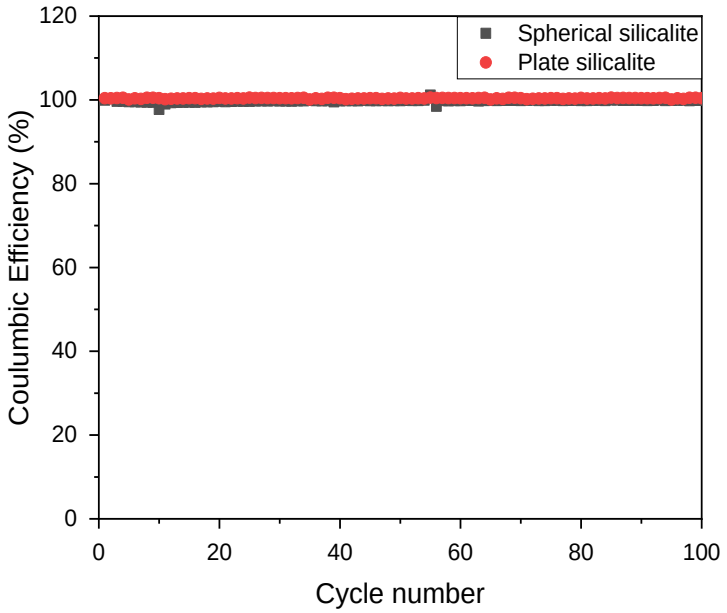

(b)

Figure 2.7. (a) CC-CV curves for charge and discharge cycles of spherical silicalite and plate silicalite separator cells at 0.2C and (b) Coulombic efficiency of the first 100 cycles for spherical and plate silicalite separator cells at 0.2C.

To analyse the rate capability of the silicalite separators at high C-rates, full cells using spherical and plate silicalite separators were tested at various C-rates of 0.5C,1C and 2C. Figure 2.8(a) shows the discharge curve for the 1st of spherical silicalite and plate silicalite separators at 0.2C,0.5C and 1C. We can see that as the C-rate increases there is significant difference in the discharge curves between spherical and plate silicalite separators.

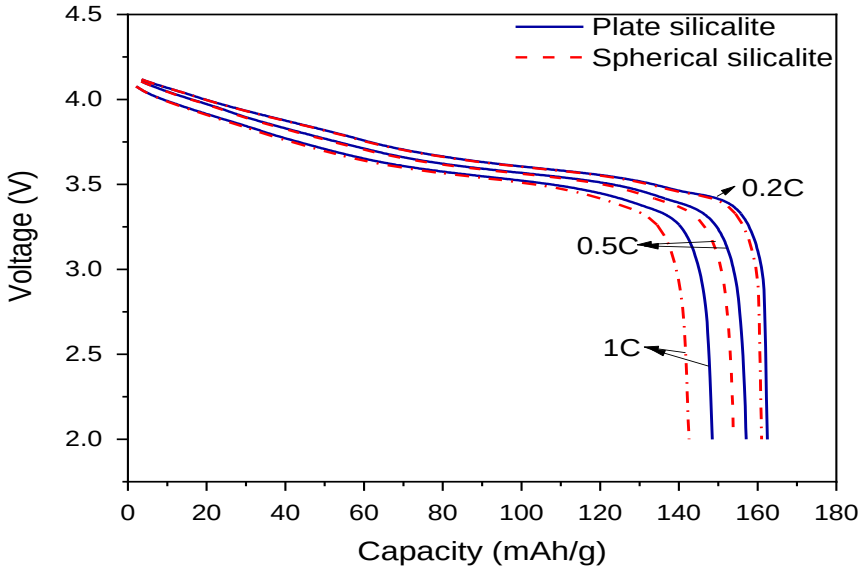

(a)

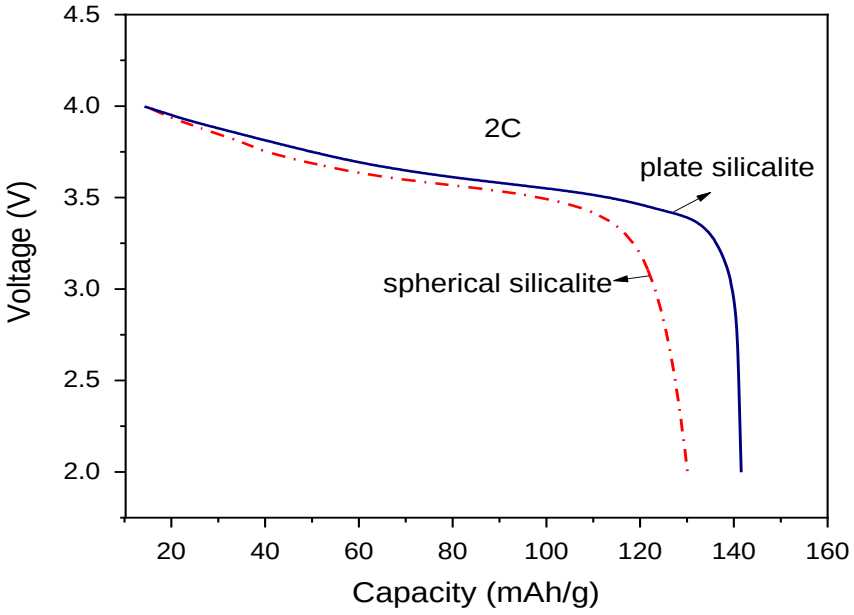

(b)

Figure 2.8. CC-CV discharge curves for plate silicalite separator and spherical silicalite separator (a) at 0.2C, 0.5C, 1C and (b) at 2C-rate.

These cells with the same configurations were again tested using the electrochemical impedance spectrometer (EIS) and the Nyquist plots for the full cells were obtained as shown in Figure 2.9. The Nyquist plots for the fully charged cells gives the impedance parameters of the ohmic resistance, SEI resistance and the charge transfer resistance after the data is fitted to the equivalent circuit using EC-Lab software. The impedance parameters are listed in Table 2.1 along with the thickness and porosity of the silicalite separators. The ohmic resistance of the cell is due to the electrolyte within the separator. The ohmic resistance of spherical silicalite (4.41 Ω) is less than plate silicalite (7.83 Ω) which is expected as spherical silicalite as better electrolyte wettability and uptake as shown in the contact angle measurement and due to higher porosity and lower tortuosity ($\tau = \sigma_{el}\ \varepsilon/\sigma$) compared to plate silicalite, spherical silicalite has lower ohmic resistance. The impedance data for spherical silicalite is consistent with the previous study done on spherical silicalite where the ohmic resistance was shown as 3.71Ω [21]. However, the SEI resistance and the charge transfer resistance of the plate silicalite separator is significantly lower than spherical silicalite separator. This is due to the uniform diffusion of the li-ions along the anode resulting in uniform and thin SEI layer formation in plate silicalite separator full cell. The plate silicalite which has higher tortuosity after compression and its lower porosity allows better electrolyte uptake of the electrodes used in the cell as compared to spherical silicalite. So, we observe different charge transfer resistance when different separators are used. Hence, we observe lower SEI resistance and charge transfer resistance in full cell using plate silicalite separator which also explains the better CC-CV cycle performance.

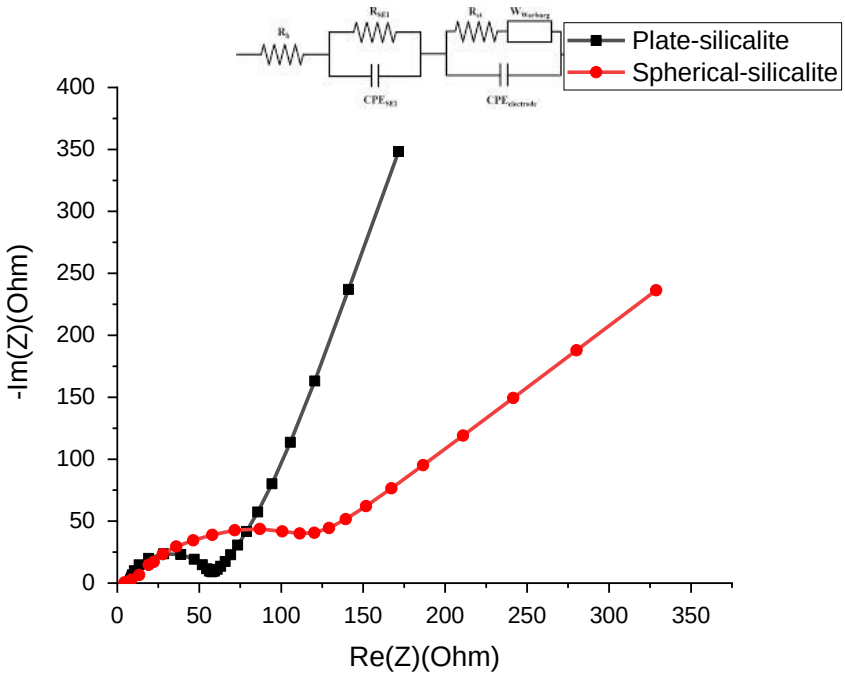

Figure 2.9. Fitted Nyquist impedance plots for full cells of spherical and plate silicalite separators.

Table 2.1 Fitted impedance parameters for full cells of spherical and plate silicalite separators.

Separator	**Thickness (μm)**	**Porosity (%)**	**Tortuosity factor**	**R_{ohm} (Ω)**	**R_{SEI} (Ω)**	**R_{ct} (Ω)**
Spherical silicalite	40	72	2.97	4.41	71.3	130.6
Plate silicalite	40	59	4.64	7.83	45.02	66.63

As the C-rate increases the solvated Li-ions in the separator tends to diffuse by tunnelling through the micropores of the plate silicalite particles rather than the inter-particle porous pathway which is more tortuous. The tunnelling of lithium ions was previously proven in the study on the diffusion of Li-ion through micropores of zeolites [55][56]. This in turn provides uniform Li-ion flux along the anode resulting in uniform and thin SEI layer. While li-ions tend to diffuse along the inter-particle pathway for the spherical silicalite separator as they as less tortuous which results in non-uniform Li-ion flux and SEI layer. This is even more apparent at a high C-rate of 2C as shown in Figure 2.8(b). This also explains the lower SEI resistance and charge transfer resistance of the plate silicalite separator.

CHAPTER 3

CONCLUSION AND RECOMMENDATIONS

3.1 Conclusions

The electrode coated silicalite separators has been coated using the blade coating method successfully on the NMC cathode. Plate silicalite separators and spherical silicalite separators have been analysed using SEM images to show the morphology and size of the particles. Plate silicalite separators have shown good electrolyte wettability similar to spherical silicalite and have good particle packing resulting in higher tortuosity. Spherical silicalite and plate silicalite separators have been used to construct cells with salt concentrated LiFSI/TMP electrolyte and they have been tested for the electrochemical performance. The plate silicalite separator has better capacity retention and rate capability with lower SEI and charge transfer resistance. This is enabled by the more uniform Li-ion flux along the anode as the li-ions diffuse along the micropores of the plate silicalite separator due to its higher tortuosity as compared to spherical silicalite separator especially at high C-rates. This results in the formation of a more uniform and thinner SEI layer which allows the plate silicalite separator to show better electrochemical performance. Hence plate silicalite separator can be used to develop li-ion cells with better cycle life, rate capability and non-flammable in nature.

3.2 Recommendations

Based on the work done in the thesis, the following are a few recommendations for future research:

1. The use of plate silicalite separator which enables a more uniform diffusion of li-ions along the anode provides as an excellent solution for the formation of

the lithium dendrites in lithium metal cells. Another property of the plate silicalite separator is its high tortuosity that can suppress the dendrite propagation across the separator compared to a less tortuous separator like the spherical silicalite separator, which also supports its choice for lithium meta cells. Hence, a study can be made on the dendrite suppression behaviour of plate silicalite separators.

2. The salt concentrated electrolyte such as the 5.3M LiFSI/TMP has excellent fire-retardant behaviour, stable and robust SEI layer and dendrite suppression ability makes it a good choice for lithium metal cells. Hence, plate silicalite can be used as the separator to compare the performance of LiFSI/TMP and regular organic electrolyte in lithium metal cells.
3. The scope of future development of lithium metal cells is solid state batteries. Here we use solid electrolytes with ceramic separator to develop lithium metal batteries. It would be an interesting study to explore the use of silicalite as the separator in solid state batteries.

REFERENCES

[1] Beard, K. W. (2019). *Linden's handbook of batteries*. McGraw-Hill Education.

[2] Deng, D. (2015). Li-ion batteries: basics, progress, and challenges. Energy Science & Engineering, 3(5), 385-418.

[3] Marom, R., Amalraj, S. F., Leifer, N., Jacob, D., & Aurbach, D. (2011). A review of advanced and practical lithium battery materials. *Journal of Materials Chemistry*, *21*(27), 9938-9954.

[4] Scrosati, B. (2000). Recent advances in lithium ion battery materials. *Electrochimica Acta*, *45*(15-16), 2461-2466.

[5] Li, Z., Huang, J., Liaw, B. Y., Metzler, V., & Zhang, J. (2014). A review of lithium deposition in lithium-ion and lithium metal secondary batteries. *Journal of power sources*, *254*, 168-182.

[6] Cheng, X. B., Zhang, R., Zhao, C. Z., & Zhang, Q. (2017). Toward safe lithium metal anode in rechargeable batteries: a review. *Chemical reviews*, *117*(15), 10403-10473.

[7] Liu, B., Zhang, J. G., & Xu, W. (2018). Advancing lithium metal batteries. *Joule*, *2*(5), 833-845.

[8] Wang, Q., Ping, P., Zhao, X., Chu, G., Sun, J., & Chen, C. (2012). Thermal runaway caused fire and explosion of lithium ion battery. Journal of power sources, 208, 210-224.

[9] Zhu, Y., Xie, J., Pei, A., Liu, B., Wu, Y., Lin, D., ... & Cui, Y. (2019). Fast lithium growth and short circuit induced by localized-temperature hotspots in lithium batteries. Nature communications, 10(1), 1-7.

[10] Abada, S., Marlair, G., Lecocq, A., Petit, M., Sauvant-Moynot, V., & Huet, F. (2016). Safety focused modeling of lithium-ion batteries: A review. Journal of Power Sources, 306, 178-192.

[11] Yuan, Y., Amine, K., Lu, J., & Shahbazian-Yassar, R. (2017). Understanding materials challenges for rechargeable ion batteries with in situ transmission electron microscopy. Nature communications, 8(1), 1-14.

[12] Ren, D., Feng, X., Lu, L., Ouyang, M., Zheng, S., Li, J., & He, X. (2017). An electrochemical-thermal coupled overcharge-to-thermal-runaway model for lithium ion battery. Journal of power sources, 364, 328-340.

[13] Wu, T., Chen, H., Wang, Q., & Sun, J. (2018). Comparison analysis on the thermal runaway of lithium-ion battery under two heating modes. Journal of hazardous materials, 344, 733-741.

[14] Feng, X., Sun, J., Ouyang, M., Wang, F., He, X., Lu, L., & Peng, H. (2015). Characterization of penetration induced thermal runaway propagation process within a large format lithium ion battery module. Journal of Power Sources, 275, 261-273.

[15] Choudhari, V. G., Dhoble, A. S., & Sathe, T. M. (2020). A review on effect of heat generation and various thermal management systems for lithium ion battery used for electric vehicle. Journal of Energy Storage, 32, 101729.

[16] Spotnitz, R., & Franklin, J. (2003). Abuse behavior of high-power, lithium-ion cells. Journal of power sources, 113(1), 81-100.

[17] Kong, L., Li, C., Jiang, J., & Pecht, M. G. (2018). Li-ion battery fire hazards and safety strategies. Energies, 11(9), 2191.

[18] Feng, X., Ouyang, M., Liu, X., Lu, L., Xia, Y., & He, X. (2018). Thermal runaway mechanism of lithium ion battery for electric vehicles: A review. Energy Storage Materials, 10, 246-267.

[19] Spinner, N. S., Field, C. R., Hammond, M. H., Williams, B. A., Myers, K. M., Lubrano, A. L., ... & Tuttle, S. G. (2015). Physical and chemical analysis of lithium-ion battery cell-to-cell failure events inside custom fire chamber. Journal of Power Sources, 279, 713-721.

[20] Wen, J., Yu, Y., & Chen, C. (2012). A review on lithium-ion batteries safety issues: existing problems and possible solutions. Materials express, 2(3), 197-212.

[21] Jiang, W., Liu, Z., Kong, Q., Yao, J., Zhang, C., Han, P., & Cui, G. (2013). A high temperature operating nanofibrous polyimide separator in Li-ion battery. *Solid State Ionics*, *232*, 44-48.

[22] Chawla, N., Bharti, N., & Singh, S. (2019). Recent advances in non-flammable electrolytes for safer lithium-ion batteries. *Batteries*, *5*(1), 19.

[23] Jiang, L., Wang, Q., Li, K., Ping, P., Jiang, L., & Sun, J. (2018). A self-cooling and flame-retardant electrolyte for safer lithium ion batteries. *Sustainable Energy & Fuels*, *2*(6), 1323-1331.

[24] Gao, T., Wang, B., Wang, L., Liu, G., Wang, F., Luo, H., & Wang, D. (2018). LiAlCl4· 3SO2 as a high conductive, non-flammable and inorganic non-aqueous liquid electrolyte for lithium ion batteries. Electrochimica Acta, 286, 77-85.

[25] Shi, P., Fang, S., Huang, J., Luo, D., Yang, L., & Hirano, S. I. (2017). A novel mixture of lithium bis (oxalato) borate, gamma-butyrolactone and non-flammable hydrofluoroether as a safe electrolyte for advanced lithium ion batteries. Journal of Materials Chemistry A, 5(37), 19982-19990.

[26] Farhat, D., Ghamouss, F., Maibach, J., Edström, K., & Lemordant, D. (2017). Adiponitrile–Lithium Bis (trimethylsulfonyl) imide Solutions as Alkyl Carbonate-free Electrolytes for Li4Ti5O12 (LTO)/LiNi1/3Co1/3Mn1/3O2 (NMC) Li-Ion Batteries. ChemPhysChem, 18(10), 1333-1344.

[27] Wang, X., Yamada, C., Naito, H., Segami, G., & Kibe, K. (2005). High-concentration trimethyl phosphate-based nonflammable electrolytes with improved charge–discharge performance of a graphite anode for lithium-ion cells. *Journal of The Electrochemical Society*, *153*(1), A135.

[28] Wang, J., Yamada, Y., Sodeyama, K., Watanabe, E., Takada, K., Tateyama, Y., & Yamada, A. (2018). Fire-extinguishing organic electrolytes for safe batteries. Nature Energy, 3(1), 22-29.

[29] Shi, P., Zheng, H., Liang, X., Sun, Y., Cheng, S., Chen, C., & Xiang, H. (2018). A highly concentrated phosphate-based electrolyte for high-safety rechargeable lithium batteries. Chemical communications, 54(35), 4453-4456.

[30] Ryou, M. H., Lee, Y. M., Park, J. K., & Choi, J. W. (2011). Mussel-inspired polydopamine-treated polyethylene separators for high-power Li-ion batteries. *Advanced materials*, *23*(27), 3066-3070.

[31] Allen, J. (2020). Review of polymers in the prevention of thermal runaway in lithium-ion batteries. Energy Reports, 6, 217-224.

[32] Eggen, C. L., McAfee, P. M., Jin, Y., & Lin, Y. S. (2015). Surface roughness and chemical properties of porous inorganic films. *Thin Solid Films*, *591*, 111-118.

[33] Yu, L., Miao, J., Jin, Y., & Lin, J. (2017). A comparative study on polypropylene separators coated with different inorganic materials for lithium-ion batteries. *Frontiers of Chemical Science and Engineering*, *11*(3), 346-352.

[34] Burriesci, N., Crisafulli, M. L., Giordano, N., Bart, J. C. J., & Polizzotti, G. (1984). Hydrothermal synthesis of zeolites from low-cost natural silica-alumina sources. Zeolites, 4(4), 384-388.

[35] Carvalho, D. V., Loeffler, N., Kim, G. T., & Passerini, S. (2015). High temperature stable separator for lithium batteries based on SiO2 and hydroxypropyl guar gum. *Membranes*, *5*(4), 632-645.

[36] Yu, L., Jin, Y., & Lin, Y. S. (2016). Ceramic coated polypropylene separators for lithium-ion batteries with improved safety: effects of high melting point organic binder. *RSC advances*, *6*(46), 40002-40009.

[37] Yu, L., Miao, J., Jin, Y., & Lin, J. (2017). A comparative study on polypropylene separators coated with different inorganic materials for lithium-ion batteries. *Frontiers of Chemical Science and Engineering*, *11*(3), 346-352.

[38] Xiang, H., Chen, J., Li, Z., & Wang, H. (2011). An inorganic membrane as a separator for lithium-ion battery. *Journal of Power Sources*, *196*(20), 8651-8655.

[39] Chen, J., Wang, S., Cai, D., & Wang, H. (2014). Porous SiO2 as a separator to improve the electrochemical performance of spinel LiMn2O4 cathode. *Journal of membrane science*, *449*, 169-175.

[40] He, M., Zhang, X., Jiang, K., Wang, J., & Wang, Y. (2015). Pure inorganic separator for lithium ion batteries. *ACS applied materials & interfaces*, *7*(1), 738-742.

[41] Raja, M., Angulakshmi, N., Thomas, S., Kumar, T. P., & Stephan, A. M. (2014). Thin, flexible and thermally stable ceramic membranes as separator for lithium-ion batteries. *Journal of membrane science*, *471*, 103-109.

[42] Sharma, G., Jin, Y., & Lin, Y. S. (2017). Lithium ion batteries with alumina separator for improved safety. *Journal of The Electrochemical Society*, *164*(6), A1184.

[43] Rafiz, K., Jin, Y., & Lin, Y. S. (2020). Performance of electrode-supported silica membrane separators in lithium-ion batteries. *Sustainable Energy & Fuels*, *4*(3), 1254-1264.

[44] Zhang, S. S. (2007). A review on the separators of liquid electrolyte Li-ion batteries. Journal of power sources, 164(1), 351-364.

[45] Xie, Y., Zou, H., Xiang, H., Xia, R., Liang, D., Shi, P., ... & Wang, H. (2016). Enhancement on the wettability of lithium battery separator toward nonaqueous electrolytes. Journal of Membrane Science, 503, 25-30.

[46] Rafiz, K., & Lin, J. Y. (2020). Safe Li-ion batteries enabled by completely inorganic electrode-coated silicalite separators. *Sustainable Energy & Fuels*, *4*(11), 5783-5794.

[47] Davis, M. E. (2002). Ordered porous materials for emerging applications. Nature, 417(6891), 813-821.

[48] De Vos, R. M., & Verweij, H. (1998). High-selectivity, high-flux silica membranes for gas separation. Science, 279(5357), 1710-1711.

[49] Lu, Y., Ganguli, R., Drewien, C. A., Anderson, M. T., Brinker, C. J., Gong, W., ... & Zink, J. I. (1997). Continuous formation of supported cubic and hexagonal mesoporous films by sol–gel dip-coating. Nature, 389(6649), 364-368.

[50] Flanigen, E. M., Bennett, J. M., Grose, R. W., Cohen, J. P., Patton, R. L., Kirchner, R. M., & Smith, J. V. (1978). Silicalite, a new hydrophobic crystalline silica molecular sieve. Nature, 271(5645), 512-516.

[51] Baerlocher, C., McCusker, L. B., & Olson, D. H. (2007). Atlas of zeolite framework types. Elsevier.

[52] Bennett, E. F. J. (1978). RW Grose JP Cohen RL Patton, RM Ktrchner and JV Srmth. *Nature (London)*, *271*, 512.

[53] Yu, M., Falconer, J. L., & Noble, R. D. (2005). Adsorption of liquid mixtures on silicalite-1 zeolite: a density-bottle method. *Langmuir*, *21*(16), 7390-7397.

[54] Zhang, X., Liu, H., & Yeung, K. L. (2006). Influence of seed size on the formation and microstructure of zeolite silicalite-1 membranes by seeded growth. *Materials chemistry and physics*, *96*(1), 42-50.

[55] Dong, X., Mi, W., Yu, L., Jin, Y., & Lin, Y. S. (2016). Zeolite coated polypropylene separators with tunable surface properties for lithium-ion batteries. *Microporous and Mesoporous Materials*, *226*, 406-414.

[56] Wang, M. Y., Han, S. H., Chao, Z. S., Li, S. Y., Tan, B., Lai, J. X., ... & Fan, J. C. (2020). Celgard-supported LiX zeolite membrane as ion-permselective separator in lithium sulfur battery. *Journal of Membrane Science*, *611*, 118386.

APPENDIX A

PREPARATION OF SPHERICAL SILICALITE POWDER

1. Add 10 g of tetraethyl orthosilicate (reagent grade 98%, Millipore Sigma), 12 g of tetra-propyl ammonium hydroxide (1M in H_2O, Millipore Sigma) and 202 g of de-ionized water to a 500ml glass beaker. A translucent to oily/opaque solution will be formed.
2. Place a clean magnetic stirrer at the bottom of the beaker and cover the beaker with paraffin wax paper.
3. Place the beaker on a magnetic stirring capable hot plate and set the temperature of the hot plate to 27 °C. Set the hot plate rpm value to 600 rpm and leave the beaker on the hot plate for ~ 20 hours.
4. Remove the beaker from the hot plate and switch off the hot plate. The solution will now have turned clear and will be transparent. Carefully transfer this solution to two 100 ml autoclaves and fill them equally with this solution.
5. Place the filled autoclave inside an oven and heat it at 130^{o}C for 8 hours. Place a hot and caution sign around the autoclave.
6. Now remove the autoclave after the oven cools down and use PPE while handling hot autoclave. Open the autoclave and drain the transparent mother liquor while preserving the white silicalite powder at the bottom of the autoclave and then remove the powder by dissolving it in de-ionized water.
7. Now, transfer this solution into a centrifuge tube and centrifuge it three times in a centrifuge at room temperature and 5,000 rpm (16.8 relative centrifugal force – (meters)). Do the centrifugation for each wash cycle for 20 minutes. Post each centrifugation cycle, the clear solution in the centrifuge tube should be drained and fresh de-ionized water should be added.

8. Finally transfer the silicalite powder and de-ionized water solution into a clean beaker and allow it to dry on a hot plate. Set the hot plate temperature at 100 °C.
9. Now take this powder and place it in an alumina crucible. Place this alumina crucible in the furnace and calcine the powder for 10 hours at 600 °C with atmospheric air as the medium. Later store the powder in a dry place.

APPENDIX B

PREPARATION OF PLATE SILICALITE POWDER

1. Add 10 g of tetraethyl orthosilicate (reagent grade 98%, Millipore Sigma), 4 g of tetra-propyl ammonium hydroxide (1M in H_2O, Millipore Sigma) and 170 g of de-ionized water to a 500ml glass beaker. A translucent to oily/opaque solution will be formed.
2. Place a clean magnetic stirrer at the bottom of the beaker and cover the beaker with paraffin wax paper.
3. Place the beaker on a magnetic stirring capable hot plate and set the temperature of the hot plate to 27 °C. Set the hot plate rpm value to 600 rpm and leave the beaker on the hot plate for ~ 20 hours.
4. Remove the beaker from the hot plate and switch off the hot plate. The solution will now have turned clear and will be transparent. Carefully transfer this solution to two 100 ml autoclaves and fill them equally with this solution.
5. Place the filled autoclave inside an oven and heat it at 155^{o}C for 10 hours. Place a hot and caution sign around the autoclave.
6. Now remove the autoclave after the oven cools down and use PPE while handling hot autoclave. Open the autoclave and drain the transparent mother liquor while preserving the white silicalite powder at the bottom of the autoclave and then remove the powder by dissolving it in de-ionized water.
7. Now, transfer this solution into a centrifuge tube and centrifuge it three times in a centrifuge at room temperature and 5,000 rpm (16.8 relative centrifugal force – (meters)). Do the centrifugation for each wash cycle for 20 minutes. Post each centrifugation cycle, the clear solution in the centrifuge tube should be drained and fresh de-ionized water should be added.

8. Finally transfer the silicalite powder and de-ionized water solution into a clean beaker and allow it to dry on a hot plate. Set the hot plate temperature at 100 °C.
9. Now take this powder and place it in an alumina crucible. Place this alumina crucible in the furnace and calcine the powder for 10 hours at 600 °C with atmospheric air as the medium. Later store the powder in a dry place.

40

APPENDIX C

PREPARATION OF SLURRY AND COATING OF SEPARATOR

1. Preparation of slurry requires the separator material in the powder form, de-ionized water and 5 wt% polyvinyl alcohol (PVA, avg. m.wt. 77,000 – 79,000).
2. To prepare PVA solution, take 5g of PVA and add it to 95g of de-ionized water and allow it to mix for 24 hours in a magnetic stirrer. The prepared PVA solution should not be older than 2 months.
3. Now to prepare the slurry, the specific amounts of powder to be mixed with PVA and water are mentioned in step 4 and step 5.
4. For the spherical silicalite - The slurry is prepared by taking 5 g of silica powder and adding it with 0.5 g of PVA and 2 g de-ionized water.
5. For the plate-shaped silicalite - The slurry is prepared by taking 2 g of silica powder and adding it with 2 g PVA and 1 g de-ionized water.
6. Add the ingredients in a glass beaker and stir the mixture manually until we get a uniform and bubble free slurry.
7. Now take a square electrode of side about 2-3 inches and place it down on a flat surface and use a clamp to make sure it does not move.
8. Take the doctor blade and adjust the caliper mounted on the doctor blade to get the required thickness (electrode + separator) of the separator to be coated on the electrode.
9. Now pour the prepared slurry on one edge of the electrode and then use the doctor blade to pull the slurry on the electrode to get the coating of desired thickness. This must be done within 5 minutes after the preparation of the slurry.

10. While using the doctor blade to coat the slurry, it must be done at a slow speed of 0.5cm/sec.
11. After the coating is done, place the electrode in the humid oven for drying at 40^{o}C and relative humidity of 60% for 24 hrs.
12. Now cut out circles of 16mm diameter from the coated electrode and then place the electrode in the vacuum oven for drying at 70^{o}C for 24 hrs.

APPENDIX D

PREPARATION OF LiFSI/TMP ELECTROLYTE

1. Place the purchased lithium bis-fluoro sulphonyl imide (LiFSI) (Kishida Chemical Corporation, Japan) and tri-methyl phosphate solvent (TMP) (reagent grade; 99.999% purity, Millipore Sigma) inside the atmosphere-controlled glovebox.
2. To prepare 5.3M LiFSI/TMP salt electrolyte, we need to calculate the mass of the salt requires to obtain 5.3M solution and mix the required mass of LiFSI salt with the calculated volume of TMP solvent. This step should be carried out inside the glove box.
3. As we do not have a weighing balance inside the glove box, we can measure the volume of the salt using a glass beaker. To obtain the appropriate volume of the salt, we can use the known value of its density (2.32g/ml) and the calculated mass required to obtain 5.3M.
4. Now open the sealed LiFSI salt container and take the calculated volume of the LiFSI salt needed to prepare 5.3M solution in a clean glass beaker. After taking the required volume of the salt in the beaker, add the calculated volume of TMP solvent to the beaker and stir the mixture until a clear solution is obtained. Let the solution rest for 24 hours.
5. All the steps needed to prepare the electrolyte are required to be carried out inside the glovebox.

APPENDIX E

OPERATION OF MERCURY POROSIMETER

1. Prepare the sample by coating the silicalite powder on the aluminium foil with the same slurry concentration as used to make the electrode-coated separator.
2. After drying the sample in the humid and vacuum oven, cut it into small rectangular pieces so that it can fit into the penetrometer.
3. Weigh the prepared sample pieces (net weight of all pieces) and then fill it inside a clean penetrometer so that it is completely full.
4. Seal the penetrometer with the cap and weigh the entire penetrometer with the sample (penetrometer mass).
5. On the mercury porosimeter laptop, on the main desktop, open the Microactive Autopore application.
6. Go to File -> New sample -> Sample description-> Material (select Garnet), Penetrometer (select s/n – (07) S Bulb,0.392 Stem, Solid) and click Edit to change Constant (enter the value on the respective penetrometer data sheet), Penetrometer mass (enter penetrometer mass), Sample mass (enter sample mass).
7. Click Analysis conditions -> No change.
8. Click Report options -> Select reports -> select all the required report options.
9. Click Save as (enter the name) -> Save.
10. Place the prepared penetrometer inside the low-pressure port. Note: make sure the degasser shows Hg drained before opening the port.
11. Make sure the nitrogen gas valve is open before the start of the experiment and the mercury level is between the maximum and minimum level. If

required refill to mercury level reach between the maximum and minimum level.

12. Go to Unit 1 -> Evacuate low pressure -> Start -> Close after it ends.
13. Go to Unit 1 -> Low pressure analysis -> Browse (select the saved file) -> Click start to run the experiment.
14. After the end of the low-pressure analysis remove the penetrometer and weigh the mass (assembly mass).
15. Now place the penetrometer inside the high-pressure port and fill it up with high pressure fluid.
16. Then close the high-pressure port and make sure there are no air bubbles present inside the port.
17. Go to Unit 1 -> High pressure analysis -> Browse (select the saved file) -> Assembly mass (enter the assembly mass) -> Click start to run the experiment.
18. After the completion of the experiment go to Reports -> Start report -> find the report saved in the folder.
19. Now remove the penetrometer from the high-pressure port and place it in a separate workspace.
20. Use the vacuum pump and syringe to remove the high-pressure fluid and mercury (if present) from the high-pressure port.
21. To clean the penetrometer, open the sealed cap while making sure that the bottom of the penetrometer is placed inside the mercury waste collecting vessel so that mercury does not spill outside.

22. Remove the sample and the mercury inside the penetrometer and put it inside the collecting vessel and clean the penetrometer thoroughly.
23. After the cleaning of penetrometer make sure the workspace is clean. Use vacuum pump to clean mercury if present.

APPENDIX F

GLOVEBOX OPERATION AND MAINTANENCE

A1. Operation of Glovebox.

1. The samples that needed to be taken inside are done through the small antechamber.
2. Fill the small antechamber with the working gas (UHP Argon) to remove the vacuum which would allow the opening of the door.
3. Now load coated NMC electrode samples into the small antechamber and turn on vacuum pump and alternately evacuate and refill the small antechamber at least 3 times.
4. Open the door of the small antechamber from the inside of the glovebox to obtain sample. Care must be taken that nitrile gloves are worn under as well as over the glovebox gloves.
5. After assembling the cell, load the samples back into the small antechamber and firmly close the door from the inside.
6. Finally purge the antechamber again 3 times and then place the antechamber in vacuum when done and at rest.

A2. Regeneration of catalyst

1. The glovebox oxygen (O2) and moisture (H2O) content must be maintained below 0.5 ppm each. To regenerate the catalyst the regeneration gas (5% UHP Hydrogen and 95% UHP Argon) is needed to start the process.
2. Make sure regeneration gas is attached and filled before attempting to begin Regeneration cycle. Then adjust the flowrate from the cylinder till 20 mm flowrate of the regeneration gas is achieved. Specially, as once started, the regeneration cycle cannot be aborted.

3. To begin regeneration cycle, click on the “REGEN” switch provided on the control panel at the top edge of the glovebox.
4. Upon clicking this switch, the display will ask “Hand valves open?”. Press down and hold the right arrow switch to toggle display from “OPEN” to “CLOSED”. Then press the “ENTER” key to confirm this position.
5. Next the display will ask “Is flow O.K.?” The display will read “NO”. Press and hold the right arrow switch to toggle display from “NO” to “YES”. Press the “ENTER” key to confirm.
6. The regeneration cycle lasts for a total of 870 minutes or 14.5 hours and cannot be aborted once the initial 10 minutes of the cycle have passed. Upon completion of the regeneration cycle, ensure that the “BLOWER” switch is switched on.

A3. Changing of catalyst in the purifier column

1. Turn off the blower and then turn off the AC power and disconnect the power line from the source.
2. Remove the wires connected to the heating element and then remove the two clamps that connect the column to the top of the column valves.
3. Disconnect the two Swagelok fittings that connect the pipes to the top of the column.
4. Now unbolt the purifier column from the floor of the glovebox. There two column inlets and note the inlet which has the catalyst material. The new material is to be added to this inlet only.

5. Then empty the entire catalyst into a waste disposal bag according to the safety standards.
6. Now add the new catalyst by adding half of the molecular sieve followed by all of the copper catalyst and then the remaining half of the molecular sieve into the inlet marked in the earlier step.
7. Reinstall the purifier column to the floor of the glovebox, noting the steps used to remove it from the above mentioned steps. Make sure the AC power line is disconnected.
8. Now connect the AC power line and restore AC power supply to the glovebox.
9. Regenerate the glovebox at least once before use.

APPENDIX G

ASSSEMBLY OF COIN CELLS

1. To construct the cell, we CR2032 type coin cell cases. Take the bottom shell of CR2032 coin cell cases.
2. Place the previously prepared and vacuum dried silicalite coated NMC cathode of 16 mm diameter in the bottom shell with separator layer facing the top side.
3. Using a pipette, add 150 µL of the prepared 5.3M LiFSI/TMP electrolyte on the separator coating layer so that the entire layer is wet with the electrolyte.
4. Now place the graphite anode of diameter 14 mm facing the soaked separator and make sure the electrode is in the centre.
5. Place two spacers on top of the graphite electrode and place one spring on top of the spacers.
6. Enclose the cell with the top shell of the CR2032 type coin cell cases and crimp the cell using the crimping machine (MSK-110, MTI) using a pressure of 400 psi.
7. Clean the exterior of the cell for any excess electrolyte that comes out during crimping

APPENDIX H

CV-CC CYCLE TESTING OF COIN CELLS

1. Place the constructed cell into the testing terminal of the battery testing machine and make sure the voltage displayed is positive. If not, reverse the cell polarity so that a positive voltage is displayed on the screen.
2. After the mounting of the cell, right click on the terminal shown on the screen and choose Single start, and then click Load to select a program suitable for the testing of the cell based on the electrode material used to construct the cell from the saved files.
3. To Make the required changes to the program for the different C-rates, change the value of the current in the program.
4. Start the cell testing at 0.1C for a couple cycles and then do testing at the required C-rates based on the experiment.
5. Calculate the active mass based on the electrode used and input the value in the program box displayed. Also change the program file name in the remarks box.
6. Select Save to save the changes and to start the cell testing.
7. After the cell testing is complete, right click on the terminal display and choose view data to see the results of the testing.
8. To save the data, select the export tab, enter a file name and click export.
9. The saved file can then be copied from the C drive for further use.
10. Before removing the cell from the terminal, right click on the terminal display and choose single stop.

APPENDIX I

ELECTROCHEMICAL IMPEDANCE SPECTROSCOPY OF COIN CELLS

1. To perform the EIS test, make sure that the cell is fully charged.
2. Now attach the sensor port and the working electrode port end to positive terminal.
3. Then attach counter electrode and reference electrode port end to negative terminal.
4. On the desktop open Powersuite application.
5. Go to Tools -> Database Management -> Create new Database. (create new folder for each run) Name of the folder and database must be identical.
6. Once database has been created, go ahead to run an experiment as follows.
7. Go to Experiment -> New -> Browse -> Open created folder.
8. Select Power sine -> single sine -> default SS -> Enter name (cannot be same as database name).
9. Click next -> No change in “Cell Definitions” -> next -> No change in “Prescan Definition” -> next -> Scan Definition.
10. Start Frequency 100 kHz, End Frequency 10 mHz, Select points per decade = 5, Rest unchanged.
11. Click next -> No change in “Advanced” -> Finish.
12. Now a test run window will appear. Check that the cell voltage is positive to ensure correct attachment of the electrode clamps.
13. Nyquist plot of main concern in test run.
14. At end of test run, select Z data, copy Z data and save in a text file.